iScience

CellPress
OPEN ACCESS

Article

Preliminary study of all-solid-state batteries: Evaluation of blast formation during the thermal runaway

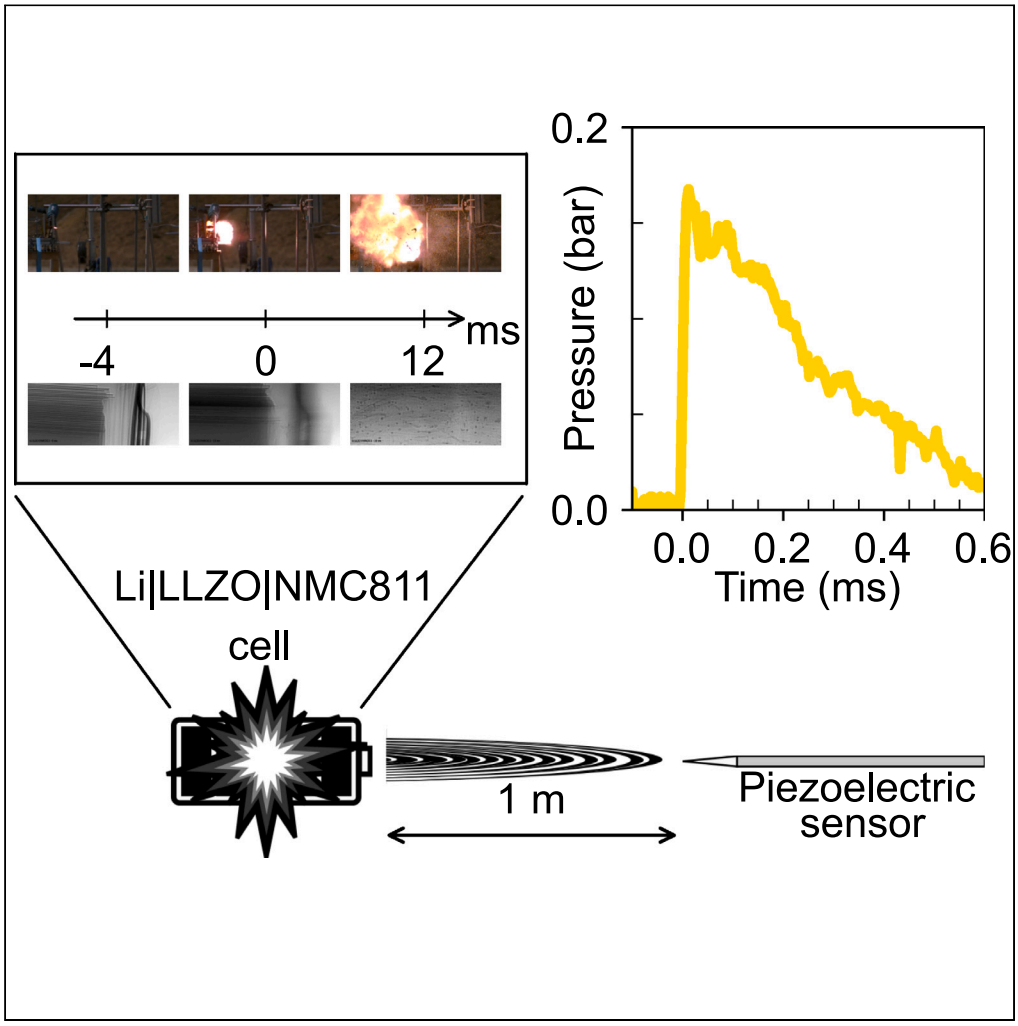

Juliette Charbonnel, Sébastien Dubourg, Etienne Testard, ..., Daniel Marteau, Pierre-Xavier Thivel, Rémi Vincent

remi.vincent@cea.fr

Highlights

The safety of the Li|LLZO|NMC811 cell has been assessed

An extremely fast thermal runaway about 5 ms is measured for Li|LLZO|NMC811 cell

A 188 mBar aerial overpressure has been measured for the Li|LLZO|NMC811 cell

Li|LLZO|NMC811 cell has a 2.7 g equivalent TNT however it is not an explosive

Charbonnel et al., iScience 26, 108078
November 17, 2023
https://doi.org/10.1016/j.isci.2023.108078

iScience

CellPress
OPEN ACCESS

Article

Preliminary study of all-solid-state batteries: Evaluation of blast formation during the thermal runaway

Juliette Charbonnel,[1,2] Sébastien Dubourg,[3] Etienne Testard,[3] Ludovic Broche,[4] Christophe Magnier,[3] Thibaut Rochard,[3] Daniel Marteau,[3] Pierre-Xavier Thivel,[2] and Rémi Vincent[1,5,*]

SUMMARY

All-solid-state batteries have been developed to increase energy density by replacing the lithiated graphite negative electrode by a lithium metal foil and to increase safety by removing the organic compounds. However, the safety issues of these batteries have received little attention up to now.

The behavior of a reassembled all-solid-state battery under thermal stress was recorded by X-ray radiography and a high-speed camera. The thermal runaway (TR) lasted about 5 ms, thus extremely fast reaction kinetics. In comparison, the TR of a lithium-ion battery is about 500 ms. Furthermore, a 188-mbar aerial overpressure was measured using a piezoelectric sensor. Although this cell is not an explosive, 2.7 g TNT equivalent was calculated for it.

This atypical behavior could have an impact on the casing or the battery pack. Therefore, it must be studied in greater detail.

INTRODUCTION

Energy sobriety is one of the major challenges that society must overcome in the near future. Reducing our dependency on fossil fuels is crucial to preserve the environment. One way of decarbonizing global power systems and the transportation sector is to develop lithium-ion batteries (LiB). LiBs are used to mitigate the intermittent production of renewable energies such as wind and photovoltaic power.[1] LiBs are also the batteries most widely used in electric vehicles. The main advantages of LiB's are their high energy density and their low self-discharge.[2]

A LiB classically consists of a stack of different materials: a positive and a negative electrode, each in contact with its respective current collector, a polymer separator, a liquid electrolyte (organic solvents and salts), and the solid-electrolyte interphase (SEI).[3] From the standpoint of risk, the polymer separator, liquid electrolyte, and SEI are considered as the most hazardous components of the LiB due to the presence of organic chemical compounds that can lead to thermal runaway (TR).[4] TR can be defined as the moment when the exothermic reaction can no longer be reversible and the increase in temperature is uncontrollable.[5] TR is characterized by the emission of toxic smoke, fire, and in some case can lead to an explosion.[6] According to Börger et al., TR starts when the following three conditions are satisfied: "the generation of heat is higher than the loss of heat," the "heat generated cannot be removed by the cooling system, causing a further increase in temperature," and the "heat increase cannot be stopped anymore by outside interference since internal heat generation releases more heat than can be removed."[7] TR ends when the ambient temperature is reached and the smoke and fire have stopped.

In all-solid-state batteries (ASSB), the polymer separator and liquid electrolyte are replaced by a ceramic or glass separator.[8] ASSB is a promising technology since it could both increase capacity and improve safety. First, in ASSB technology, the graphite negative electrode is substituted by a lithium metal foil. This enables drastically increasing the specific energy from 250 to 500 $Wh \cdot kg^{-1}$.[9,10] Secondly, the melted lithium in contact with the ceramic separator, $Li_7La_3Zr_2O_{12}$ (LLZO), is thermally stable up to 350°C whereas a standard polymer separator for LiB like polyethylene (PE) reacts at 140°C.[11–13] Therefore, ceramic and glass separators drastically increase the thermic stability of ASSB. Furthermore, the compressive Young's modulus of LLZO is about 150 GPa.[14] By comparison, the compressive Young's modulus of PE, a standard separator for LiB, is about 1 GPa.[15] Theoretically, a ceramic separator with a Young's modulus higher than 6 GPa like LLZO could eliminate the growth of lithium dendrites and thus prevent the perforation of the separator.[16] Lithium dendrites have been observed at the interphase between lithium metal foil and the LLZO separator.[17] Hence, lithium dendrites can be a safety risk for the ASSB if the porosity of the ceramic layer is not fully controlled. In addition, organic compounds are considered as another risk factor that could lead to TR.[4] Therefore,

[1]University Grenoble Alpes, CEA, LITEN, DEHT, 38000 Grenoble, France
[2]University Grenoble Alpes, University Savoie Mont Blanc, CNRS, Grenoble INP, LEPMI, 38000 Grenoble, France
[3]CEA/Le Ripault, BP 16, 37260 Monts, France
[4]European Synchrotron Radiation Facility (ESRF), 38000 Grenoble, France
[5]Lead contact
*Correspondence: remi.vincent@cea.fr
https://doi.org/10.1016/j.isci.2023.108078

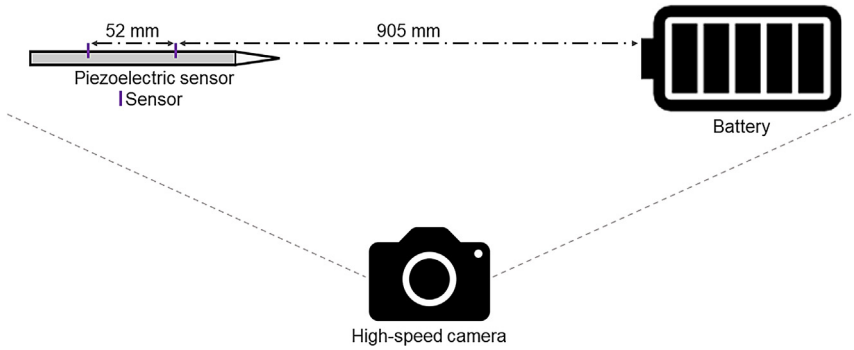

Figure 1. Set-up for blast wave measurement

the absence of organic compounds in ASSB should minimize the risk of TR. Nonetheless, Feng et al. used a pouch cell with $LiNi_{1/3}Mn_{1/3}Co_{1/3}O_2$ and $LiM\ n_2O_4$ (1:1)-based positive electrodes and MAG-10 graphite-based negative electrodes. The cell was charged with a state of charge (SOC) of 100%. The liquid electrolyte and/or the polymer separator were removed from this cell. Despite this absence, TR was recorded by the ARC test.[18] Another study demonstrated that even without liquid electrolyte, polymer separator and SEI TR takes place.[19] It seems that the absence of organic compounds does not completely prevent the triggering of TR.

Currently, ASSB is not a mature technology. The problems encountered are the unsuitability of the material and control over the interface. All common solid electrolytes have at least one major drawback limiting the development of viable ASSB and must be improved in the future to outperform LiB.[9] Lastly, production costs must be reduced to ensure industrial viability.[20] ASSB safety has been studied only marginally, with most scientific communications on ASSB focusing mainly on material synthesis/properties, the positive electrode interface, the lithium electrode interface and theory/modeling.[9] In their studies, Johnson and Bates modeled an 18650 cell and a large format cell TR, respectively, and showed that TR occurs in both cases.[21,22] ASSB seems to be safer under external overheating. However, in the case of short-circuit or catastrophic solid electrolyte failure, ASSB could lead to TR with dramatic consequences.[22] Another TR model has been developed for a Li|LLZO|Li_yCoO_2 cell. This simulation showed an onset temperature of about 300°C and a maximum temperature of about 1030°C.[21] Furthermore, characterisations of materials have been performed to estimate the safety of ASSB.[19,23] Differential scanning calorimetry (DSC) analyses of the materials making up ASSB show a maximal molar enthalpy of 200 kJ mol^{-1}.[23] Therefore, TR may occur. Finally, an 18,650 graphite (Gr)/silicon (SiO_x)|LLZO| $LiNi_{0.8}Mn_{0.1}Co_{0.1}O_2$ (NMC811) cell was reassembled in all-solid-state. The initiation temperature (T_{ini}) and maximum temperature (T_{max}) were found to be close to those of LiB. The energy released was only 11% lower.[19]

For the purpose of this study, a bespoke cell was designed to assess the safety issues of a Li|LLZO|NMC811 cell at SOC 100. This cell has an open circuit voltage (OCV) of 4.2 V between the electrodes (3 Ah). An SOC 100 was chosen to assess worst-case safety. The negative electrode was a 50-μm lithium metal foil, which is representative of the lithium usually introduced into ASSB.[24,25] The interfaces between both the electrodes and LLZO were not optimized. Therefore, the electrochemical characterisations could not be performed because of the high internal resistance. As this paper focuses on materials and their thermal behavior and not on their electrochemical characteristics, the non-optimization of interfaces is not dealt with here.

Two techniques were used to characterize the TR of the Li|LLZO|NMC811 cell. High-speed X-ray radiography was used to visualize the very rapid evolution of the cell's internal structures during TR. Then open-air overpressure measurements were performed to qualify the effect of this rapid kinetic by air shock wave characterisation.

Firstly, high-speed X-ray radiography is used to observe the internal behavior of the cell during TR.[26] It allows observing jelly roll collapse the formation of gas pockets and ejections of particles by wave.[19] It helps to understand the damage suffered by the casing.[27] The most at-risk areas leading to powerful TR were also identified.[28] The set up used to contain the TR during the X-ray analysis was described more precisely in our previous study.[19] The beamline ID19 was used at the European Synchrotron Radiation Facility (ESRF) to record the internal behavior of the Li|LLZO|NMC811 cell. The same set-up was used to measure the energy released, the pressure and the duration of TR. It is used to simultaneously record external measurements (temperatures and pressure) and the internal behavior of the Li|LLZO|NMC811 cell during TR.

Secondly, specific pressure sensors commonly used for blast wave observation were used since an extremely short rising time is needed to precisely depict the pressure discontinuity encountered at the shock front. It is crucial to characterize the shock wave and their effects on both structures and persons because it could be devastating.[29,30] The comparison between the TR of a LiB cell and TNT has already been proposed by Shan et al.[31–33] This comparison was mainly based on the energy released during the event with a ratio of 1 g of TNT equivalent to 4.184 kJ. Furthermore, Kinney and Graham suggested calculating the TNT equivalent for explosives by measuring the suppression peak to qualify the formation of a shock wave and its mechanical impact.[34] Open-air overpressure measurements were performed at the shooting range operated by CEA (Figure 1).

These techniques were used to compare the TR behavior of LGHG2 and Li|LLZO|NMC811 cells.

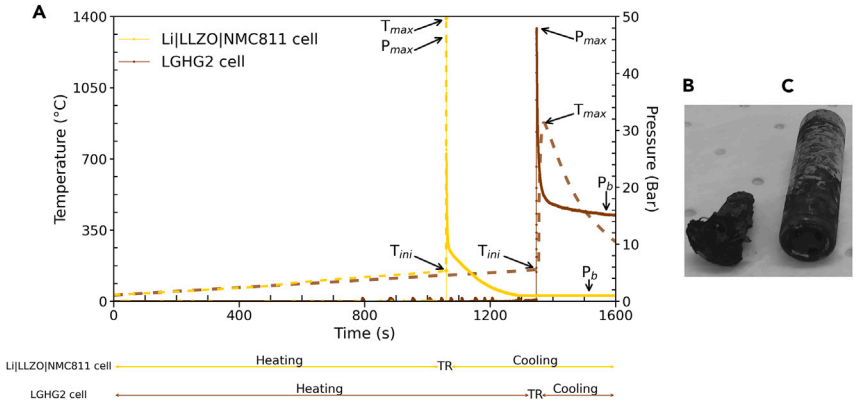

Figure 2. Li|LLZO|NMC811 cell and LGHG2 cell at SOC 100

(A) Time course of the pressure (solid line with circle marker) and the battery surface temperature (dash line) in the set-up.

(B) Li|LLZO|NMC811 casing after TR and (C) LGHG2 casing after TR.

RESULTS

Thermal runaway characteristics

The set-up described in a previous article was used to characterize the TR of Li|LLZO|NMC811 and LGHG2 cells.[19] This set-up was used to measure the surface temperature of the cell and the pressure induced by the gases released during TR (Figure 2A). The thermal abuse takes place in three steps. The first represents the heating of the cell with a temperature ramp of 6°C per minute[35] (Figure 2A—heating phase). During the heating phase, the pressure remains constant and the temperature increases linearly up to the initiation temperature (T_{ini}). The second step corresponds to TR (Figure 2A—TR phase). At this stage, the temperature and the pressure increase sharply up to T_{max} and P_{max}. The last step, the cooling phase, the pressure drops to the balancing pressure (P_b) and the ambient temperature (T_{amb}). In addition, Figures 2B and 2C show the visual aspect of the two batteries after TR.

It is noteworthy that the maximal temperature for the Li|LLZO|NMC811 cell could not be recorded. Indeed, the maximal temperature reached by the Li|LLZO|NMC811 cell must be higher than 1,370°C, the maximal temperature that TC can record. Furthermore, the casing of Li|LLZO|NMC811 cell was made of nickel-plated steel. It can melt if the temperature reaches at least 1,400°C. Therefore, considering the appearance of the ASSB cell after TR (Figure 2B), the maximal temperature reached by the Li|LLZO|NMC811 cell can be estimated at around 1,400°C. The pressure and temperature curves for the LGLH2 cell are similar to those of the Li|LLZO|NMC811 cell. The LGHG2 cell reached the same pressure as the Li|LLZO|NMC811 cell. However, its maximal temperature was at least about two times lower, reaching about 880°C.

The behavior of the LGHG2 cell was similar to that of our previous study, demonstrating good data repeatability across the experimental setup. Therefore, the experiments could be replicated with a good reliability. Furthermore, from the macroscopic standpoint the behavior of the two cells was comparable. It is by studying more precisely the specific parameters of TR such as the maximum temperature, the volume of gas released and the reaction kinetics that the striking differences can be highlighted.

Cell observation by X-Ray radiography

When TR is triggered (Figure 2A, phase TR), the pressure and the temperature reach their maximum values. To characterize the cell's internal reaction during TR, high-speed X-ray radiography was used. As shown in the previous paper, only an element of volume of the cell is observed.[19] To our knowledge, this is the first time that a TR of ASSB made of a lithium metal negative electrode (Li|LLZO|NMC811) has been observed. Figure 3 shows the X-ray radiographies and the illustrations of Li|LLZO|NMC811 cell at 100% of SOC during TR. The X-ray radiographies were extracted from the Video S1, which is the whole record of the Li|LLZO|NMC811 cell during TR.

On X-ray radiography, TR starts when cell materials start to react and TR ends when all cell materials are ejected from the cell. At the start of TR, the electrochemical assembly layers (Li + LLZO + NMC811) move and swell at $t_{ini+10ms}$ (Figures 3B and 3F). At $t_{ini+13ms}$, the positive pole turns off. It should be noted that the electrochemical assembly layers are still in the casing when the positive pole turns off (Figures 3C and 3G). The electrochemical assembly layers are ejected from the cell only one millisecond later (Figure 3H). Finally, at $t_{ini+20ms}$, traces of solidified product on the inside of the setup are observable. These traces come from a large part of the product melted by the TR (Figure 3D).

As previously reported, during TR, the LGHG2 cell reacted from the center to the outer layers over a period of approximately 400 ms.[19] Contrary to expectation, the reaction did not occur from the center to the outer layers for the Li|LLZO|NMC811 cell. All the layers seemed to react simultaneously and abruptly. Furthermore, the evacuation of the first particle and the delamination of the electrodes were not observed for this cell. Finally, referring to the literature, the reaction kinetics of the Li|LLZO|NMC811 cell appeared to be one of the fastest among LiBs.

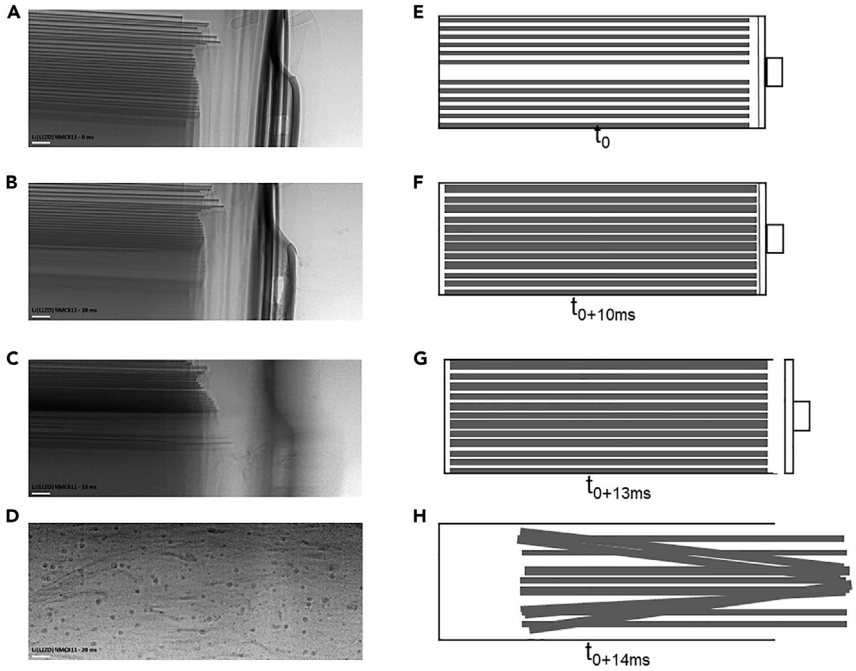

Figure 3. Li|LLZO|NMC811 cell at SOC 100 during TR

X-ray radiographies at (A) t_{ini}, (B) $t_{ini+10ms}$ moveing and swelling of electrochemical assembly layers, (C) $t_{ini+13ms}$ positive pole turns off, and (D) $t_{ini+20ms}$ traces come from the large part of the product melted. Illustrations of the internal behavior: (E) the cell before TR, (F) electrodes moving and swelling, (G) positive pole turns off, and (H) particle wave ejection. The bar gives the 2 ± 0.1 mm scale. The gray rectangles represent the electrochemical assembly layer (Li + LLZO + NMC811). Video S1.

Quantitative analyses

TR parameters were recorded such as skin temperature and pressure using the set-up sensors. During TR, the instantaneous volume of gas released V (m^3) was calculated from the instantaneous internal pressure P (Pa) measurements (Equation 1). P_{atm} (Pa) and V_{cal} (m^3) are respectively the atmospheric pressure and the calorimeter volume.

$$V = \frac{P}{P_{atm}} \cdot V_{cal} \quad \text{(Equation 1)}$$

Then, the volumetric flow rate $\dot{V}$ ($m^3 \cdot s^{-1}$) was determined from instantaneous volume variation ΔV (m^3) divided by the time variation Δt (s).

$$\dot{V} = \frac{\Delta V}{\Delta t} \quad \text{(Equation 2)}$$

By plotting the volumetric flow rate against time from the moment T_{ini} is reached (Figure 4), the behavior of the LGHG2 cell shows a progressive increase of internal reaction rate, contrary to the Li|LLZO|NMC811 cell which had an abrupt behavior. For the Li|LLZO|NMC811 cell, the X-ray radiographies show a dazzling TR (Figure 3) and the volumetric flow rate increases swiftly in a few milliseconds (Figure 4). In addition, the TR time was about 4 ms for the Li|LLZO|NMC811 cell. It was 80 times faster than that of the LGHG2 cell (around 329 ms). The maximal volumetric flow rate of Li|LLZO|NMC811 was about 10,000 L s^{-1}, i.e., 60 times higher than that of the LGHG2 cell.

Another way to study the behavioral differences between the LGHG2 cell and the Li|LLZO|NMC811 cell is to observe their casing after TR. For the LGHG2 cell, the casing was undamaged (Figure 2C). Only the vent opened during TR. In contrast, little was left of the Li|LLZO|NMC811 casing (Figure 2B). The nickel-plated steel casing melted during TR. The reaction between the melted lithium and the oxygen released by the positive electrode produced Li_2O.[36] This reaction could release enough energy to melt the casing.

One way to compare the TR behavior of different technologies is to plot the maximum temperature against the initiation temperature. Figure 5A shows this comparison based on results from the literature and our studies. The LiB with NCA as positive electrode,[37–39] the LGHG2 cell[19] and the Gr/SiO_x|LLZO|NMC811 cell[19] have similar maximal and initiation temperatures. The LFP cell has a higher initiation temperature and a lower maximal temperature.[40–42] The Li|LLZO|NMC811 cell has the same initiation temperature as the NCA, LGHG2, and Gr/SiO_x|LLZO|NMC811 cells. However, their maximal temperature is at least twice as high. On calorimetry tests, TR starts when 5% of P_{max} is reached and TR ends when 95% of P_{max} is reached. Based on the same principle, the amounts of gas produced (mmol) were plotted against the TR duration (ms) for the same different LiB technologies (Figure 5B). The duration of TR was about 4 ms for the Li|LLZO|NMC811 cell, i.e.,

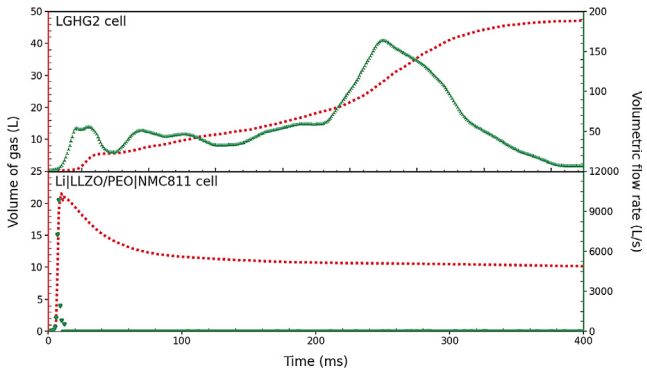

Figure 4. Time course of the volume of gas (red dash line) and the volumetric flow rate (green solid line) during TR of LGHG2 cell and Li|LLZO|NMC811 cell, here $t_0 = t_{T_{ini}}$

40 times faster than the Gr/ SiO_x |LLZO|NMC811 cell and 90 times faster than the LGHG2 cell. The amount of gas released for Li|LLZO|NMC811 cell during TR was about 35 mmol, i.e., 5 times lower than the Gr/SiO_x |LLZO|NMC811 cell and 7 times lower than the LGHG2 cell. The presence of a greater quantity of combustible product in the cell (graphite, separator, solvent) seemed to reduce the reaction kinetics and increase the quantity of gas. The increase in the quantity of gas could be explained by thermal degradation and partial combustion of the combustible products. Likewise, it can be considered that the partial combustion caused by a greater quantity of combustible than oxidant decreased the reaction kinetics. Finally, an energy released of 82 kJ by the Li|LLZO|NMC811 cell was measured by the calorimeter developed for high-speed X-ray radiography.[19]

Overpressure measurements

The very fast reaction kinetics and the characteristics of the TR seen in Video S1, allowed considering the formation of a shock wave during the Li|LLZO|NMC811 cell explosion. In order to further analyze the behavior of the all-solid state cell, overpressure measurements were performed. One striking similarity between the overpressure/time curves of both explosives and the Li|LLZO|NMC811 cell undergoing TR was the clear pressure discontinuity that appeared with the shock front (Figure 6A). This sharp pressure variation demonstrates that an extremely fast-paced reaction took place in the Li|LLZO|NMC811 cell with the potential to produce a shock wave in the air. The overpressure wave generated was slightly supersonic, close to 370 m s^{-1}.

For explosive reactions in air, Kinney and Graham established a well-known scaling law and tabulated peak overpressure, pressure impulse and other pressure wave parameters.[34] This scaling law is based on the use of the reduced distance (Z) equal to real distance, d (m) from the center of the explosion divided by the cubic root of the explosive mass, m (kg) (TNT equivalent) (Equation 3).

$$Z = \frac{d}{m^{\frac{1}{3}}} \quad \text{(Equation 3)}$$

Using the measured distance between pressure sensors and the TNT equivalent mass used for the three trials with explosive, the results were compared with values computed from the scaling law (Figure 6B). The peak overpressures measured were in good agreement with the computed values. Small differences can be explained in part by the specificity of our setup. Tabulated values should be predictive for freely propagating shock waves from spherical charges.

In order to obtain a TNT equivalent mass for Li|LLZO|NMC811 cells, a random mass was initially given to each cell which gave the first value of Z and the corresponding tabulated pressure. The mass was then optimized to minimize the error between the tabulated and measured overpressures across the four sensors. This value was about 2.7 g for the Li|LLZO|NMC811 cell.

The shock wave was also observable on the high-speed camera recording Videos S2 due to the modification of the air refractive index generated by the blast with both explosive and Li|LLZO|NMC811 cell samples. The duration of the event was less than 0.2 ms with the explosive and 0.8 ms with the Li|LLZO|NMC811 cell while TR usually takes place in hundreds of milliseconds with LiBs (Video S3).

Attempts were made to measure the overpressure produced by the LGHG2 battery but ended up being inconclusive, as they did not produce shock waves in air. The gas production rate of LiB was much too slow to be noticeable in an open-air measurement setup.

Finally, we can also notice in the additional Videos S2 and S3 that the device for holding the Li|LLZO|NMC811 cell is severed then projected in the air during the explosion while it remains perfectly in place for the LGHG2 cell.

DISCUSSION

Three specific methods were implemented. Firstly, ASSB were reconstituted with a lithium metal foil negative electrode, an LLZO solid separator and a NMC811-based positive electrode removed from LGHG2 cell. Secondly, the TR of Li|LLZO|NMC811 was recorded by X-ray radiographies at the ESRF. Thirdly, a specific assembly was developed to measure the shock wave.

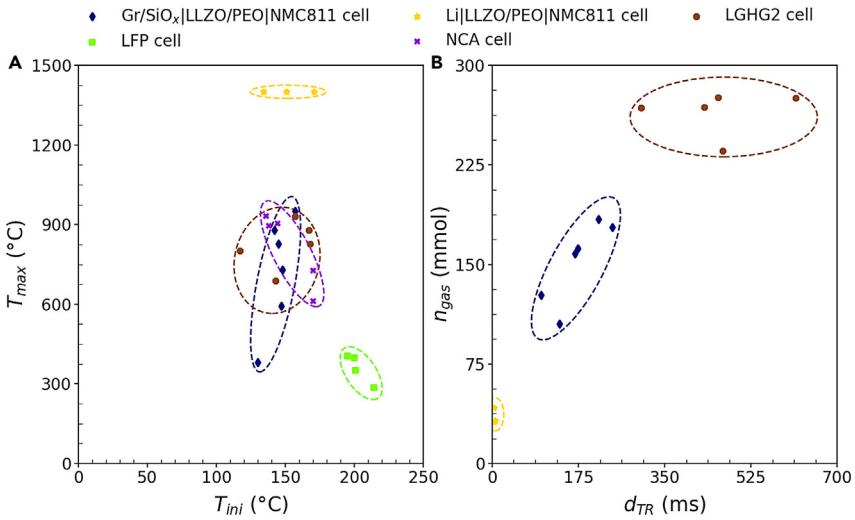

Figure 5. Plot for LiB with a positive electrode in NCA and LFP, for the LGHG2 cell, for the Gr/SiO$_x$|LLZO/PEO|NMC811 cell and the Li|LLZO|NMC811 cell

(A) The maximal temperature (T_{max}) versus the initial temperature (T_{ini}), and (B) the amount of gas (n_{gas}) versus the duration of TR (d_{TR}).

The TR of the Li|LLZO|NMC811 cell, which was recorded at the ESRF, demonstrated an atypical behavior in comparison with a traditional LiB. Its reaction kinetics was 100 times faster than LiB. Contrary to the LiB TR, which presented a fast continuous runaway like a wick from the center to the outer layers, the Li|LLZO|NMC811 cell presented a brutal reaction of all the layers simultaneously.

As a result of these tests, one question remained unanswered: could the Li|LLZO|NMC811 cell detonate and generate an overpressure wave?

The specific assembly developed to measure shock waves showed that the Li|LLZO|NMC811 cell generated a shock wave, contrary to the LGHG2 cell. A rigorous methodology was implemented to measure blast waves and to determine a TNT equivalent.

Previous attempts to correlate the LiB explosion observed during TR to a TNT equivalent mass have been published.[31–33] According to our study, during TR the LGHG2 and Li|LLZO|NMC811 cells both released about 80 kJ of energy. As, by definition, 1 g of TNT is equivalent to 4.184 kJ then both cells should have a TNT equivalent of about 19 g and the same behavior. However, in our study, an aerial shock front was observed for the Li|LLZO|NMC811 cell, contrary to the LGHG2 cell. Therefore, their behaviors were considerably different. Furthermore, the TNT equivalent of the Li|LLZO|NMC811 cell was experimentally estimated at about 2.7 g, i.e., seven times lower than with the energy method. This difference is an important point because it shows that although the Li|LLZO|NMC811 cell produced a shock wave during its TR only a small part of the chemical energy was converted into a shock wave. Thus, for 80 kJ of thermal reaction, a LiBs cell did not convert the energy into a shock wave, whereas the Li|LLZO|NMC811 cell converted the equivalent of 2.7 g of TNT, i.e., 11.4KJ. Although Li|LLZO|NMC811 cells are not explosive, it is important to accurately assess the impact of the shock wave formed on the surrounding mechanical structures. Therefore, it would be better to estimate a TNT equivalent from an aerial shock front rather than the energy released during TR.

Contrary to LiB, the Li|LLZO|NMC811 cells generated a shock wave; however, they produced much less gas than LiB. Therefore, the effect on the battery pack casing was not easy to demonstrate. However, in supplementary Videos S2 and S3, it can be noted that the difference in runaway regime between the two cell types leads to a drastically different impact on the cell support. In the case of Li|LLZO|NMC811 cell the support is severed, then ejected, whereas it remains perfectly in place for the LGHG2 cell.

Moreover, the X-ray radiography tests and the measure of blast wave were two different tests, providing redundant information. The very fast reaction kinetics measured for the Li|LLZO|NMC811 cell in the closed X-ray set-up allowed concluding that a shock wave forms without a significant supply of oxygen from the ambient air.

Although it was not easy to demonstrate the impact of the Li|LLZO|NMC811 cell TR on the casing of the battery pack, it will be important to study it in the future as these first results show that it can be very different from that of LIB cells.

Conclusion

In this study, we showed that in the presence of lithium as negative electrode and despite the absence of organic materials (liquid electrolyte, polymer separator, or SEI), the TR kinetics of a reassembled ASSB is much faster than that of a LiB.

For the first time, with two different methods, open-air overpressure and high speed X-ray measurements, the formation of a shock wave was demonstrated during the TR of representative reassembled ASSB cells. The TR of a 3 Ah reassembled ASSB cell was able to induce an aerial shock wave of about 188 mBar one meter away from the cell. Based solely on the peak overpressure produced and taking in consideration the specificity of our testing conditions, this 3 Ah cell could generate an effect similar to 2.7 g of TNT.

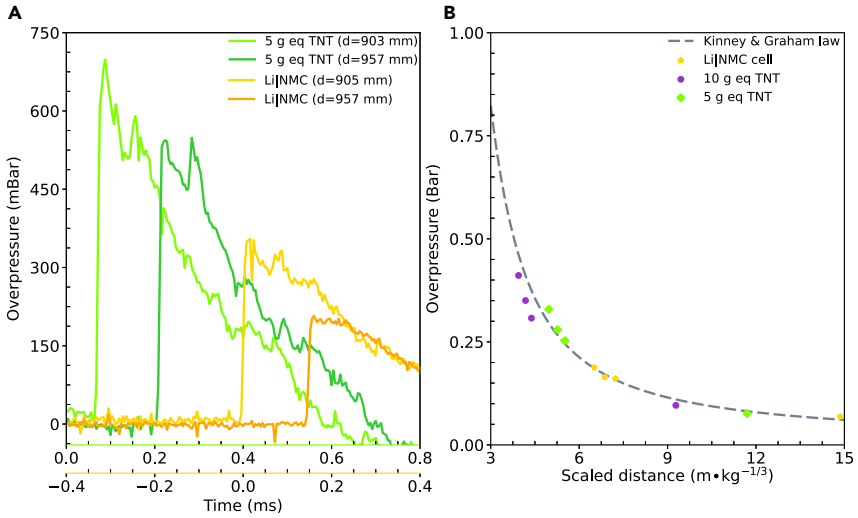

Figure 6. Comparison of aerial overpressure measurements between commercial explosive and Li|LLZO|NMC811 cell

(A) $t_{0ms} = t_{T_{ini}}$ for the Li|LLZO|NMC811 cell and $t_{0.4ms} = t_{explosion\ trigger}$ 5 g eq. TNT of commercial explosive. Distances shown in the upper right corner are from the cell/explosive charge to the sensing element of the pressure sensor.

(B) Peak overpressure as a function of scaled distance. The purple circles, the green diamond and the yellow stars represent the 10 g eq. TNT, the 5 g eq. TNT and the Li|LLZO|NMC811 cell respectively.

The air overpressure method was a more reliable method than the energy method for determining the TNT equivalent in this particular case, as measuring the energy released did not take into account the kinetics of the reaction. Although the suppression value gives an indication, it is not easy to directly quantify on the destructive capabilities of the cells, e.g., on the battery pack casing. Nevertheless, this new TR regime could generate additional difficulties for the management of TR propagation and the dimensioning of the battery pack casing. Further tests need to be carried out to better assess the safety of these cells and more broadly of lithium metal and unstable cathode cells such as NMC811.

In order to reach high energy densities, ASSB have to use lithium-metal foil as a negative electrode. In order to achieve fast charges without the risk of short circuits induced by dendrites, lithium metal foils should preferably be used with a ceramic or a glass separator. For this type of technology, the technical development of electrochemically efficient solutions is a major issue. However, the supplementary constraints regarding safety linked to the use of lithium-metal foil should not be neglected.

ASSBs seem to be a promising technology from the standpoint of electrochemical energy storage, but the safety aspect must be addressed and taken into account in future studies. In particular, the reaction pathways and their kinetics, which lead to TR of LiB and more specifically of ASSB, should be studied.

Limitations of the study

Currently, it is hard to obtain several ampere-hour all-solid-state batteries. Therefore, it is complicated to verify their safety. To assess the safety of all-solid-state batteries, reassembled all-solid-state cells were manufactured from commercial cells. One limitation is the representativeness of this reassembled cell because it is not electrically active and the interfaces are not optimized. However, all the components are in the same conditions than an ASSB charged at SOC 100 (the positive electrode is delithiated).

STAR★METHODS

Detailed methods are provided in the online version of this paper and include the following:

- KEY RESOURCES TABLE
- RESOURCE AVAILABILITY
  - Lead contact
  - Material availability
  - Data and code availability
- METHOD DETAILS
  - Li|LLZO|NMC811 cell preparation
  - Beamline description
  - Closed set-up
  - Blast wave measurement

- QUANTIFICATION AND STATISTICAL ANALYSIS
  - Radiography data processing

SUPPLEMENTAL INFORMATION

Supplemental information can be found online at https://doi.org/10.1016/j.isci.2023.108078.

ACKNOWLEDGMENTS

The authors would like to express their gratitude for the technical support provided by Pierre Balfet, David Brun-Buisson, Jérôme Cognard, Lise Daniel, Kamel Bachir Elezaar, and Magali Reytier for the abuse tests, and by Elise Gutel and Christophe Vincens for solid-state manufacturing.

We also thank the Grenoble Battery Hub's Long Term Project "Multi-scale Multi-techniques investigations of Li-ion batteries: toward a European Battery Hub" (pilot proposal no. MA4929) for recording the X-ray radiographies.

The closed setup was developed by CEA with financial support from the European Union under the Horizon 2020 research and innovation program (TEESMAT project grant agreement No. 814106).

AUTHOR CONTRIBUTIONS

R. V., J.C., and P-X.T. conceptualization; J.C., R.V., E.T., and S.D. data curation and formal analysis; R.V. funding acquisition; J.C., L.B., S.D., C.M., T.R., and D.M. investigation; R.V., L.B., and S.D. methodology and resources; J.C., R.V., P-X.T., E.T., and S.D. validation and visualization; J.C., R.V., L.B., E.T., and S.D. writing - original draft. All authors reviewed and edited the article.

DECLARATION OF INTERESTS

The authors have a patent related to this work.

INCLUSION AND DIVERSITY

One or more of the authors of this paper self-identifies as a gender minority in their field of research.

Received: June 14, 2023
Revised: September 5, 2023
Accepted: September 25, 2023
Published: September 28, 2023

REFERENCES

1. Thango, B.A., and Bokoro, P.N. (2022). Battery Energy Storage for Photovoltaic Application in South Africa: A Review. Energies *15*, 5962. https://doi.org/10.3390/en15165962.
2. Andre, D., Kim, S.-J., Lamp, P., Lux, S.F., Maglia, F., Paschos, O., and Stiaszny, B. (2015). Future generations of cathode materials: an automotive industry perspective. J. Mater. Chem. A *3*, 6709–6732. https://doi.org/10.1039/C5TA00361J.
3. Nitta, N., Wu, F., Lee, J.T., and Yushin, G. (2015). Li-ion battery materials: present and future. Mater. Today *18*, 252–264. https://doi.org/10.1016/j.mattod.2014.10.040.
4. Tian, X., Yi, Y., Fang, B., Yang, P., Wang, T., Liu, P., Qu, L., Li, M., and Zhang, S. (2020). Design Strategies of Safe Electrolytes for Preventing Thermal Runaway in Lithium Ion Batteries. Chem. Mater. *32*, 9821–9848. https://doi.org/10.1021/acs.chemmater.0c02428.
5. Wang, Q., Ping, P., Zhao, X., Chu, G., Sun, J., and Chen, C. (2012). Thermal runaway caused fire and explosion of lithium ion battery. J. Power Sources *208*, 210–224. https://doi.org/10.1016/j.jpowsour.2012.02.038.
6. Zalosh, R., Gandhi, P., and Barowy, A. (2021). Lithium-ion energy storage battery explosion incidents. J. Loss Prev. Process. Ind. *72*, 104560. https://doi.org/10.1016/j.jlp.2021.104560.
7. Börger, A., Mertens, J., and Wenzl, H. (2019). Thermal runaway and thermal runaway propagation in batteries: What do we talk about? J. Energy Storage *24*, 100649. https://doi.org/10.1016/j.est.2019.01.012.
8. Tian, Y., Zeng, G., Rutt, A., Shi, T., Kim, H., Wang, J., Koettgen, J., Sun, Y., Ouyang, B., Chen, T., et al. (2021). Promises and Challenges of Next-Generation "Beyond Li-ion" Batteries for Electric Vehicles and Grid Decarbonization. Chem. Rev. *121*, 1623–1669. https://doi.org/10.1021/acs.chemrev.0c00767.
9. Albertus, P., Anandan, V., Ban, C., Balsara, N., Belharouak, I., Buettner-Garrett, J., Chen, Z., Daniel, C., Doeff, M., Dudney, N.J., et al. (2021). Challenges for and Pathways toward Li-Metal-Based All-Solid-State Batteries. ACS Energy Lett. *6*, 1399–1404. https://doi.org/10.1021/acsenergylett.1c00445.
10. Schneider, S.F., Bauer, C., Novák, P., and Berg, E.J. (2019). A modeling framework to assess specific energy, costs and environmental impacts of Li-ion and Na-ion batteries. Sustain. Energy Fuels *3*, 3061–3070. https://doi.org/10.1039/C9SE00427K.
11. Wolfenstine, J., Allen, J.L., Read, J., and Sakamoto, J. (2013). Chemical stability of cubic Li7La3Zr2O12 with molten lithium at elevated temperature. J. Mater. Sci. *48*, 5846–5851. https://doi.org/10.1007/s10853-013-7380-z.
12. Song, K.W., and Kim, C.K. (2010). Coating with macroporous polyarylate via a nonsolvent induced phase separation process for enhancement of polyethylene separator thermal stability. J. Membr. Sci. *352*, 239–246. https://doi.org/10.1016/j.memsci.2010.02.020.
13. Chen, R., Nolan, A.M., Lu, J., Wang, J., Yu, X., Mo, Y., Chen, L., Huang, X., and Li, H. (2020). The Thermal Stability of Lithium Solid Electrolytes with Metallic Lithium. Joule *4*, 812–821. https://doi.org/10.1016/j.joule.2020.03.012.
14. Pang, M.-C., Yang, K., Brugge, R., Zhang, T., Liu, X., Pan, F., Yang, S., Aguadero, A., Wu, B., Marinescu, M., et al. (2021). Interactions are important: Linking multi-physics mechanisms to the performance and degradation of solid-state batteries. Mater. Today *49*, 145–183. https://doi.org/10.1016/j.mattod.2021.02.011.
15. Li, R., He, Y., Qin, W., Zhang, Z., Su, J., Guan, Q., Chen, Y., and Jin, L. (2022). Effect of external pressure and internal stress on battery performance and lifespan. Energy Storage Mater. *36*, 395–404. https://doi.org/10.1016/j.ensm.2022.07.034.

16. Keller, M., Varzi, A., and Passerini, S. (2018). Hybrid electrolytes for lithium metal batteries. J. Power Sources *392*, 206–225. https://doi.org/10.1016/j.jpowsour.2018.04.099.
17. Meda, U.S., Lal, L., Sushantha, M., Garg, P., and Garg, P. (2022). Solid Electrolyte Interphase (SEI), a boon or a bane for lithium batteries: A review on the recent advances. J. Energy Storage *47*, 103564. https://doi.org/10.1016/j.est.2021.103564.
18. Feng, X., Zheng, S., Ren, D., He, X., Wang, L., Cui, H., Liu, X., Jin, C., Zhang, F., Xu, C., et al. (2019). Investigating the thermal runaway mechanisms of lithium-ion batteries based on thermal analysis database. Appl. Energy *246*, 53–64. https://doi.org/10.1016/j.apenergy.2019.04.009.
19. Charbonnel, J., Darmet, N., Deilhes, C., Broche, L., Reytier, M., Thivel, P.-X., and Vincent, R. (2022). Safety Evaluation of All-Solid-State Batteries: An Innovative Methodology Using In Situ Synchrotron X-ray Radiography. ACS Appl. Energy Mater. *5*, 10862–10871. https://doi.org/10.1021/acsaem.2c01514.
20. Schnell, J., Knörzer, H., Imbsweiler, A.J., and Reinhart, G. (2020). Solid versus Liquid—A Bottom-Up Calculation Model to Analyze the Manufacturing Cost of Future High-Energy Batteries. Energy Technol. *8*, 1901237. https://doi.org/10.1002/ente.201901237.
21. Johnson, N., and Albertus, P. (2022). Modeling Thermal Behavior and Safety of Large Format All-Solid-State Lithium Metal Batteries under Thermal Ramp and Short Circuit Conditions. J. Electrochem. Soc. *169*, 060546. https://doi.org/10.1149/1945-7111/ac79cf.
22. Bates, A.M., Preger, Y., Torres-Castro, L., Harrison, K.L., Harris, S.J., and Hewson, J. (2022). Are solid-state batteries safer than lithium-ion batteries? Joule *6*, 742–755. https://doi.org/10.1016/j.joule.2022.02.007.
23. Inoue, T., and Mukai, K. (2017). Are All-Solid-State Lithium-Ion Batteries Really Safe?–Verification by Differential Scanning Calorimetry with an All-Inclusive Microcell. ACS Appl. Mater. Interfaces *9*, 1507–1515. https://doi.org/10.1021/acsami.6b13224.
24. Delaporte, N., Perea, A., Collin-Martin, S., Léonard, M., Matton, J., Gariepy, V., Demers, H., Clément, D., Rivard, E., and Vijh, A. (2022). High Performance Lithium Metal Anode with a Nanolayer of LiZn Alloy for All-Solid-State Batteries. Batter. Supercaps *5*, e202200245. https://doi.org/10.1002/batt.202200245.
25. Lu, B., Bao, W., Yao, W., Doux, J.-M., Fang, C., and Meng, Y.S. (2022). Editors' Choice—Methods—Pressure Control Apparatus for Lithium Metal Batteries. J. Electrochem. Soc. *169*, 070537. https://doi.org/10.1149/1945-7111/ac834c.
26. Finegan, D.P., Scheel, M., Robinson, J.B., Tjaden, B., Hunt, I., Mason, T.J., Millichamp, J., Di Michiel, M., Offer, G.J., Hinds, G., et al. (2015). In-operando high-speed tomography of lithium-ion batteries during thermal runaway. Nat. Commun. *6*, 6924. https://doi.org/10.1038/ncomms7924.
27. Finegan, D.P., Darcy, E., Keyser, M., Tjaden, B., Heenan, T.M.M., Jervis, R., Bailey, J.J., Vo, N.T., Magdysyuk, O.V., Drakopoulos, M., et al. (2018). Identifying the Cause of Rupture of Li-Ion Batteries during Thermal Runaway. Adv. Sci. *5*, 1700369. https://doi.org/10.1002/advs.201700369.
28. Finegan, D.P., Darst, J., Walker, W., Li, Q., Yang, C., Jervis, R., Heenan, T.M., Hack, J., Thomas, J.C., Rack, A., et al. (2019). Modelling and experiments to identify high-risk failure scenarios for testing the safety of lithium-ion cells. J. Power Sources *417*, 29–41. https://doi.org/10.1016/j.jpowsour.2019.01.077.
29. Held, M. (1983). TNT — Equivalent. Propellants, Explos. Pyrotech. *8*, 158–167. https://doi.org/10.1002/prep.19830080507.
30. Malhotra, A., Carson, D., and McFadden, S. (2017). Blast pressure leakage into buildings and effects on humans. Procedia Eng. *210*, 386–392.
31. Shan, T., Wang, Z., Zhu, X., Wang, H., Zhou, Y., Wang, Y., Zhang, J., and Sun, Z. (2022). Explosion behavior investigation and safety assessment of large-format lithium-ion pouch cells. J. Energy Chem. *72*, 241–257. https://doi.org/10.1016/j.jechem.2022.04.018.
32. Lu, T.-Y., Chiang, C.-C., Wu, S.-H., Chen, K.-C., Lin, S.-J., Wen, C.-Y., and Shu, C.M. (2013). Thermal hazard evaluations of 18650 lithium-ion batteries by an adiabatic calorimeter. J. Therm. Anal. Calorim. *114*, 1083–1088. https://doi.org/10.1007/s10973-013-3137-9.
33. LIU, Q., ZHU, Q., ZHU, W., YI, X., and HAN, X. (2022). Thermal Runaway Characteristics of 18650 NCM Lithium-ion Batteries under the Different Initial Pressures. Electrochemistry *90*, 87004. https://doi.org/10.5796/electrochemistry.22-00049.
34. Kinney, G., and Graham, K. (1985). Explosive Shocks in Air, 2nd edition (Springer-Verlag), p. 282.
35. RTCA Minimum Operational Performances Standards for Rechargeable Lithium Battery and Battery Systems (DO-311) (2017 (RTCA DO-311).
36. Xu, X.-Q., Cheng, X.-B., Jiang, F.-N., Yang, S.-J., Ren, D., Shi, P., Hsu, H., Yuan, H., Huang, J.-Q., Ouyang, M., and Zhang, Q. (2022). Dendrite-accelerated thermal runaway mechanisms of lithium metal pouch batteries. SusMat *2*, 435–444. https://doi.org/10.1002/sus2.74.
37. Golubkov, A.W., Scheikl, S., Planteu, R., Voitic, G., Wiltsche, H., Stangl, C., Fauler, G., Thaler, A., and Hacker, V. (2015). Thermal runaway of commercial 18650 Li-ion batteries with LFP and NCA cathodes – impact of state of charge and overcharge. RSC Adv. *5*, 57171–57186. https://doi.org/10.1039/C5RA05897J.
38. Chombo, P.V., and Laoonual, Y. (2022). Prediction of the onset of thermal runaway and its thermal hazards in 18650 lithium-ion battery abused by external heating. Fire Saf. J. *129*, 103560. https://doi.org/10.1016/j.firesaf.2022.103560.
39. Zhao, C., Sun, J., and Wang, Q. (2020). Thermal runaway hazards investigation on 18650 lithium-ion battery using extended volume accelerating rate calorimeter. J. Energy Storage *28*, 101232. https://doi.org/10.1016/j.est.2020.101232.
40. Yuan, L., Dubaniewicz, T., Zlochower, I., Thomas, R., and Rayyan, N. (2020). Experimental study on thermal runaway and vented gases of lithium-ion cells. Process Saf. Environ. Protect. *144*, 186–192. https://doi.org/10.1016/j.psep.2020.07.028.
41. Duh, Y.-S., Theng, J.-H., Chen, C.-C., and Kao, C.-S. (2020). Comparative study on thermal runaway of commercial 14500, 18650 and 26650 LiFePO4 batteries used in electric vehicles. J. Energy Storage *31*, 101580. https://doi.org/10.1016/j.est.2020.101580.
42. Golubkov, A.W., Fuchs, D., Wagner, J., Wiltsche, H., Stangl, C., Fauler, G., Voitic, G., Thaler, A., and Hacker, V. (2014). Thermal-runaway experiments on consumer Li-ion batteries with metal-oxide and olivin-type cathodes. RSC Adv. *4*, 3633–3642. https://doi.org/10.1039/C3RA45748F.
43. Somerville, L., Bareño, J., Jennings, P., McGordon, A., Lyness, C., and Bloom, I. (2016). The Effect of Pre-Analysis Washing on the Surface Film of Graphite Electrodes. Electrochim. Acta *206*, 70–76. https://doi.org/10.1016/j.electacta.2016.04.133.

STAR★METHODS

KEY RESOURCES TABLE

REAGENT or RESOURCE	SOURCE	IDENTIFIER
Chemicals, peptides, and recombinant proteins		
Dimethyl carbonate	Sigma-Aldrich	CAS: 615-38-6
LLZO: $Li_7La_3Zr_2O_{12}$	Nanomyte from NEI corporation	NANOMYTE® SOX-25
PEO: Poly(ethylene oxide)	Sigma-Aldrich	CAS: 25322-68-3
Acetonitrile	Sigma-Aldrich	CAS: 75-05-8
Hexomax	#NA	#NA
Deposited data		
Inition temperatures of LiB with a positive electrode in NCA	https://doi.org/10.1039/C5RA05897J https://doi.org/10.1016/j.firesaf.2022.103560 https://doi.org/10.1016/j.est.2020.101232	#NA
Maximal temperatures of LiB with a positive electrode in NCA	https://doi.org/10.1039/C5RA05897J https://doi.org/10.1016/j.firesaf.2022.103560 https://doi.org/10.1016/j.est.2020.101232	#NA
Inition temperatures of LiB with a positive electrode in LFP	https://doi.org/10.1016/j.psep.2020.07.028 https://doi.org/10.1016/j.est.2020.101580 https://doi.org/10.1039/C3RA45748F	#NA
Maximal temperatures of LiB with a positive electrode in LFP	https://doi.org/10.1016/j.psep.2020.07.028 https://doi.org/10.1016/j.est.2020.101580 https://doi.org/10.1039/C3RA45748F	#NA
Inition temperatures, duration of thermal runaway and quantity of gas released of a Gr/SiO_x|LLZO|NMC811 cell	https://doi.org/10.1021/acsaem.2c01514	#NA
Maximal temperatures, duration of thermal runaway and quantity of gas released of a Gr/SiO_x|LLZO|NMC811 cell	https://doi.org/10.1021/acsaem.2c01514	#NA
Software and algorithms		
ImageJ 1.53	#NA	#NA
Other		
HG2 cell	LG	#NA

RESOURCE AVAILABILITY

Lead contact

Further information and requests for resources should be directed to and will be dealt with by the lead contact, Rémi Vincent (remi.vincent@cea.fr).

Material availability

This study did not generate new material.

Data and code availability

The data that support the findings of this study are available from the corresponding author upon reasonable request.

METHOD DETAILS

Li|LLZO|NMC811 cell preparation

A commercial 18650-type cell (LGHG2) was discharged at 0% of SOC. The next steps happened in a glove box whose oxygen and water rates were lower than 0.1 mg L^{-1}. The negative pole was drilled with a 0.6 mm drill. The drilled cell was charged up to 100 % of SOC, i.e. 4.2 V and 1.5 A with a 50 mA end-current. Then, the drilled and charged cell was placed in an oven at 70°C 48 h. This stage evaporated the liquid organic

electrolyte and prevented the deterioration of the component. The internal resistance was measured constantly to monitor the evaporation. The positive electrode was removed from the casing and separated from the polymer separator and the negative electrode. The positive electrode as washed twice for 3 minutes with dimethyl carbonate (DMC) to remove $LiPF_6$ salt and the SEI.[43]

The LLZO ink was composed of 21% LLZO (Nanomyte from NEI corporation), 4% PEO (300,000 $g \cdot mol^{-1}$ from Sigma-Aldrich) and 75% acetonitrile (99.8% anhydrous from Sigma-Aldrich). This ink was manufactured in anhydrous room at room temperature (dew point at −40°C). LLZO and PEO are dried in an oven at 55°C for 48 h. A dispersing device (Dispermat LC) was used to grind-mix efficiently the ink components for at least 10 minutes.

The positive electrode was coated in an anhydrous room. A film applicator (Elcometer 4340) was used to apply the LLZO ink with a 40 μm gap size. The coated electrode (NMC811 positive electrode removed from LGHG2 cell) was placed under an extractor fan for 12 h.

The coated positive electrode (NMC811|LLZO/PEO) was wrapped with a self-supporting lithium foil in anhydrous room at room temperature. The jelly roll was placed inside a nickel steel casing. The cell was crimped with a vent, a joint and a positive pole. The Li|LLZO|NMC811 cell is obtained with a 3 Ah capacity.

Beamline description

The synchrotron beam was produced by a 150 wiggler magnet with a large band spectrum. A mean x-ray energy of 81 keV was reached by removing low energies with 2.8 mm aluminium and 1.4 mm copper filters. An optical system including two similar top-down Hasselblad lenses was used to achieve a magnification of 1. The native pixel size of the Photron FAST-CAM SA4 camera of 20 μm gave an effective resolution of 20 μm. X-rays were transformed into visible light through a 1 mm thick LuAg scintillator.

Closed set-up

A thermally insulated and airtight closed system was used as the set-up. This calorimeter can be split into two parts. One with a 25.4 mm diameter stainless-steel tube large enough to contain an 18650-type cell and at the same time allows X-rays to pass through the 2.1 mm thick wall of tube. The other with a 50.8 mm diameter stainless-steel tube to prevent TR overpressure from increasing the volume. Moreover, a 100 bar safety valve was added to manage an overpressure event if necessary.

A 0.32 mm diameter heating wire was wound around the cell tested. This wire was connected to a 300 V and 9 A power supply. Overheating was induced by a constant heating power at $6\ °C \cdot min^{-1}$. Polytetrafluoroethylene (PTFE) adhesive tape was used to electrically isolate the cell, the heating wire and the stainless-steel set-up. Temperature was recorded each 500 ms with thermocouples (TC). Nine of them were located on the set-up and two were located on the middle of the cell. Pressure was recorded each 1 ms with a 100 Bar pressure sensor.

Blast wave measurement

The setup consisted of a lightweight support made with extruded aluminium beams 1 m high. Explosive samples were made of an empty casing similar to ASSB filled with a commercial explosive: Hexomax. The explosive was cut and weighed beforehand and shaped to fill the inside of the casing. Three explosive samples were tested with a TNT equivalent mass of 0.84 g, 6 g and 12 g, respectively. A commercial detonator was used to trigger the explosive.

ASSB samples consisted of bespoke cells on which a 0.35 μm NiCr heating wire was wrapped tightly. Overheating was induced by a 1.5 A constant current.

The cylindrical casing was placed on top of the support, its axis parallel to the ground. Three pen-style pressure sensors from Piezotronics were placed at the same height as the charge or cell close to its axis (with a slight offset to prevent disturbance from one sensor to another) at various distances from the samples (between 90 and 220 cm). One of the pressure sensors was equipped with two sensing elements placed 10 cm apart, thus totalling four measures.

The high-speed camera (Photron FAST-CAM SA4 model 500K-C2) was placed perpendicularly to the positive terminal in order to observe the gases and ejecta. A speed of 5000 fps was chosen as a trade-off between speed and image resolution with an acquisition time of 70 ms for a total of 351 images for the Li|LLZO|NMC811 cell and with an acquisition time of 321.8 ms for a total of 1610 images for the LGHG2 cell.

QUANTIFICATION AND STATISTICAL ANALYSIS

Radiography data processing

ImageJ 1.53 was used to process the X-ray radiographies. The "Image calculator divide" function was adopted to remove all the imperfections linked to the high-speed camera and the stainless-steel calorimeter. Two functions, "Enhance Contrast" and "Enhance Local Contrast", were used to adjust radiography contrast and brightness. A text tool was used to add the timer indicator. For the movies, an arrow tool was used to show the phenomena of interest. The "avi" file extension was run to compile images in the movie.